NO SURPRISE FOR PERSEVERANCE: AN IGNEOUS ENVIRONMENT IN JEZERO CRATER, MARS, IS AN EXPECTED OUTCOME OF ISIDIS BASIN LOADING. P. J. McGovern (3600 Bay Area Blvd., Houston, TX 77058; mcgovern@lpi.usra.edu), Lunar and Planetary Institute/USRA.

Introduction: Stunning and unexpected findings have been reported by the Perseverance Rover in Jezero Crater at the margin of the Isidis Basin on Mars! A sedimentary setting at the Perseverance landing site and environs was predicted based on geomorphic reasoning applied to remote sensing datasets. Instead, Perseverance found igneous basement and a pervasively volcanic environment, with abundant evidence of intrusive materials [e.g., 1, 2], While perhaps a surprise geologically, such associations are an expected result of a magma ascent-enhancing lithospheric stress state induced by a spherical shell response to broad-scale loads such as those filling the Isidis Basin [e.g., 3].

The stress state in the lithosphere exerts a primary control on magma ascent, through principal stress orientations dictating the orientations of magma transporting bodies (dikes and sills) and by vertical gradients of stress governing the pressure distributions in dikes (see Eqn. 1). Numerous analyses have considered the influence of one or both of these conditions in controlling magma ascent pathways around large lithospheric loads in diverse planetary settings as on the Moon [4-8], Mars [9], Io [10], and Pluto [11]. Further, loading of spherical shells excites a monopole membrane (stretching) response that when superposed with the dipole flexure (bending) response creates an environment particularly suitable for magma ascent in regions surrounding large loads [6-8, 10-11].

Modeling Technique: To examine scenarios for enhancement of magma ascent in Jezero crater and more generally the circum-Isidis region, we create Finite Element Method (FEM) models of the lunar lithosphere in COMSOL Multiphysics FEM package. Our 2-dimensional spherical shell models use an FEM mesh in axisymmetric geometry (Fig. 5) for computational efficiency. The models calculate stresses and deformations of the entire lithosphere, and within the basin-filling load, which acts effectively as a local stiffening of the lithosphere. For the case in Fig. 5, this stiffening is offset by lithospheric thinning below the basin, reflecting thermally weakened material below the basin center, a remnant of the impact process [e.g., 12]. We used a flat-bottomed "super Gaussian" load profile to resemble observations of relatively "fresh" or "pristine" basins and the results of hydrocode impact models [12]. The basin is filled to its (initial) brim with a load of density = 2800 kg/m^3, appropriate for basaltic material and above the lower bound established by [3], to reflect likely contributions of volcanic materials.

Magma ascent criteria. Two stress-based magma ascent criteria can be applied, assuming transport in vertical dikes: 1) A stress orientation criterion, requiring that the least compressive stress be oriented horizontally to allow vertical dikes to form [13]. 2) A stress gradient criterion, that can be derived from the equation for ascent velocity u_z in a dike [14]:

$$u_z = (1/3\eta)\, w^2\, (d\Delta\sigma_T/dz + \Delta\rho g + d\Delta P/dz) \qquad (1)$$

where $\Delta\sigma_T$ is the difference of horizontal and vertical normal stresses, $\Delta\rho$ is the rock-magma density contrast, g is gravity, w is dike width, η is viscosity, and $d\Delta P/dz$ is the gradient of magmatic overpressure (neglected). The FEM loading stresses give us the first term which can be equated to the second term (buoyancy) to calculate the "effective buoyant density" $\Delta\rho_{efb}$ required to offset negative buoyancy of basalt in less mafic crust.

Results: The effects of lithospheric stress gradients (see Eqn. 1) on magma ascent through the lithosphere are shown in Figs. 1 and 2. For most of the lithosphere, radial normal stress σ_r is in horizontal compression (greyed out in Fig. 1), thereby violating our first ascent criterion, but in one prominent region of the upper lithosphere beyond the load, σ_r is in horizontal extension and the stress gradients predict $\Delta\rho_{efb}$ values of up to 300 kg/m^3, indicating a great enhancement of magma ascent at the basin margin. The region of potential magma enhancement extends from 100 km within the basin margin to several 100s of km beyond this margin. This finding comports with evidence for enhanced volcanic activity at these distances from the center of Isidis Basin, including the detection of widespread volcanic basement at Jezero Crater [1-2], the pervasive signal of olivine (presuming magmatic transport) around Nili Fossae [15], and the presence of the Syrtis Major volcanic shield [16].

One difficulty stems from the lack of such a favorable environment in the lower lithosphere, thanks to the expected lower lithosphere compression [e.g., 17]. However, consideration of the out-of-plane horizontal stress component, σ_{op}, reveals that the first ascent criterion is satisfied throughout the thickness of the lithosphere (Fig. 2) because of an extensional membrane stress generated in the spherical shell [7, 8, 11]. While the values of $\Delta\rho_{efb}$ driven by σ_{op} are significantly lower (20-30 kg/m^3) than those for σ_r (Fig. 7), σ_{op} has the advantage of driving magma ascent through the lower lithosphere in dikes with radial orientations (Fig. 2), whereas magma ascent through dikes of circumferential orientations is barred in the lower lithosphere (Fig. 1). This finding implies a multiple-stage ascent scenario for magmas in locations at the Isidis rim like Nili Fossae and Syrtis Major: initial

ascent through the lower lithosphere in radially oriented dikes (perpendicular to the least compressive σ_{op} component, Fig. 2), and then switching to the much more favorable environment of circumferential dikes in the upper lithosphere (Fig. 1). This scenario could favor the formation of mid-lithosphere magma storage bodies, perhaps like the subsurface chambers inferred from gravity analysis at Syrtis Major [16]. Such systems could account for the evidence for cumulates and other igneous materials found by Perseverance [1, 2].

References: [1] Wiens et al. (2022) Mars, Sci. Adv. 8, eabo3399. [2] Y. Liu et al., (2022) Science 10.1126/science.abo2756. [3] Ritzer, J. A., and S. A. Hauck, II, (2009) *Icarus, 201*, 528-539. [4] Solomon S. C. and Head J. W. (1979) *JGR, 84*, 1667. [5] Solomon S. C. and Head J. W. (1980) *Rev. Geophys. and Space Phys., 18*, 107. [6] McGovern P. J. and Litherland M. M. (2011) *LPS XLII*, Abstract # 2587. [7] Andrews-Hanna, J. C., et al. (2014) *Nature, 514,* doi:doi:10.1038/nature13697. [8] Michaut, C. et al. (2020), Earth Planet. Sci. Lett., 530, 115889. [9] McGovern, P. J., and S. C. Solomon (1993) *J. Geophys. Res., 98*, 23,553-23,579. [10] McGovern P. J. et al. (2016) Icarus, 272, 246-257. [11] McGovern P.J., et al. (2021) *J. Geophys. Res.,* 126, e2021JE006964. [12] Potter R.W.K., et al. (2013) *Journal of Geophysical Research - Planets*, 118:5, 963-979. [13] Anderson, E. M., (1951). *The Dynamics of Faulting and Dyke Formation with Applications to Britain*, Oliver and Boyd, Edinburgh, 2nd ed., 206 pp., 1951. [14] Rubin A.M. (1995) *Annual Rev. Earth Planet. Sci.* 23, 287-336. [15] Tornabene, L. L., et al. (2008) *J. Geophys. Res., 113*, E10001, doi:10.1029/2007JE002988. [16] Lillis, R. J., et al. (2015), *J. Geophys. Res.*, 120, 1476–1496, doi:10.1002/2014JE004774. [17] McGovern, P. J., et al. (2013) *J. Geophys. Res., 118*, doi:10.1002/2013JE004455, 2013. [18] Simpson, R. W. (1997) *J. Geophys. Res., 102*, 17,909-17,919.

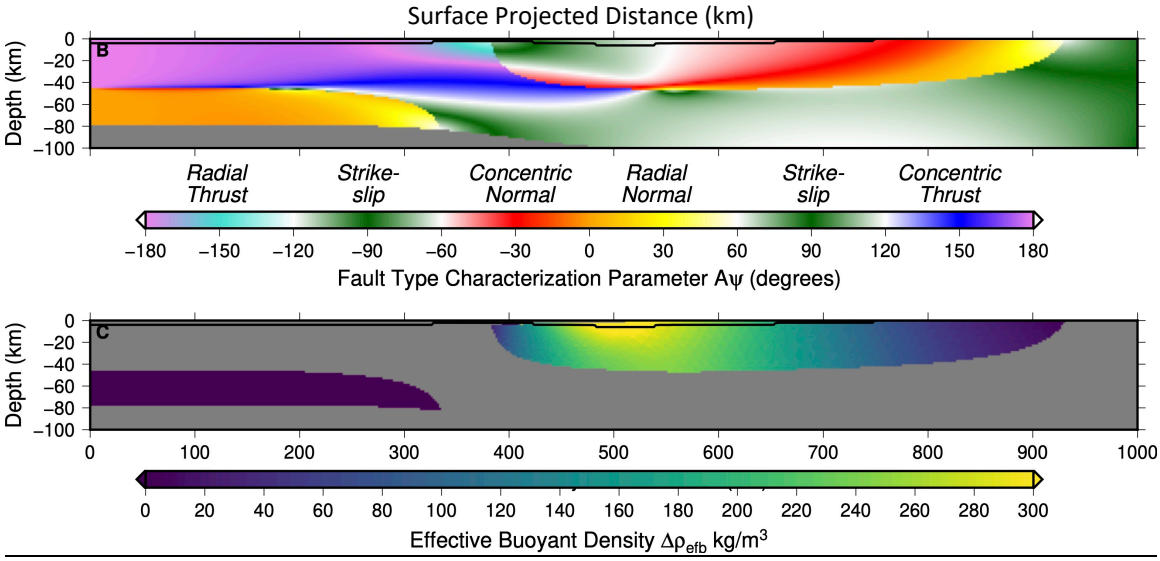

Figure 1. State of stress in an FEM model of the Martian lithosphere subject to loading by infill of a flat-floored impact basin. The model uses spherical shell geometry, but the results are projected according to the distance along the spherical surface above any given point for compactness. Top Plot: Cross-sectional map of the shape parameter $A\psi$ of [18]. "Pure" fault regime labels are given above the color scale. Solid black contours correspond to $P_f = 1$, bounding regions inside which a Mohr–Coluomb failure criterion is satisfied. The region lacking elements due to impact-induced lithosphere thinning is shown in gray. Bottom Plot: Effective buoyant density $\Delta\rho_{efb}$ calculated from vertical gradient of the radial tectonic stress $d\Delta\sigma_T/dz = d(\sigma_r - \sigma_z)/dz$. Regions for which σ_r is not the most extensional stress (i.e., where the stress orientation criterion for radial diking is not met) are masked out by grey.

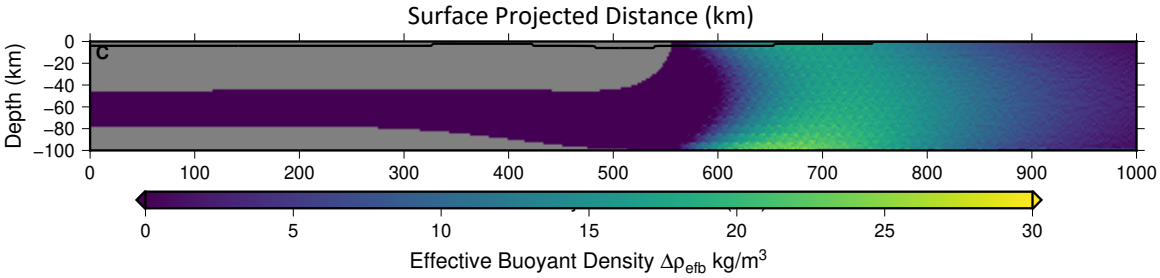

Figure 2. As in Fig. 1 (bottom), with $\Delta\rho_{efb}$ calculated for the vertical gradient of out-of-plane horizontal stress σ_{op}.